THE EUROPEAN
PHYSICAL JOURNAL C

Testing leptoquark/EFT in $\bar{B} \to D^{(*)} l \bar{\nu}$ at the LHC

Syuhei Iguro[1]**, Michihisa Takeuchi**[2]**, Ryoutaro Watanabe**[3,4,a]

[1] Department of Physics, Nagoya University, Nagoya 464-8602, Japan
[2] Kobayashi-Maskawa Institute for the Origin of Particles and the Universe, Nagoya University, Nagoya 464-8602, Japan
[3] INFN, Sezione di Roma Tre, Via della Vasca Navale 84, 00146 Rome, Italy
[4] INFN, Sezione di Pisa, Largo B. Pontecorvo 3, 56127 Pisa, Italy

Abstract We investigate the current LHC bounds on New Physics (NP) that contributes to $\bar{B} \to D^{(*)} l \bar{\nu}$ for $l = (e, \mu, \tau)$ by considering both leptoquark (LQ) models and an effective-field-theory (EFT) Hamiltonian. Experimental analyses from l + missing searches with high p_T are applied to evaluate the NP constraints with respect to the Wilson coefficients. A novel point of this work is to show difference between LQs and EFT for the applicable LHC bound. In particular, we find that the EFT description is *not* valid to search for LQs with the mass less than $\lesssim 10\,\text{TeV}$ at the LHC and leads to overestimated bounds. We also discuss future prospects of high luminosity LHC searches including the charge asymmetry of background and signal events. Finally, a combined summary for the flavor and LHC bounds is given, and then we see that in several NP scenarios the LHC constraints are comparable with the flavor ones.

1 Introduction

The flavor studies of the semi-leptonic B decay processes have been developed these years to test the electroweak sector of the Standard Model (SM) and also to look for evidence of New Physics (NP) effects. In particular, the charged current is described as

$$\mathcal{H}_{\text{eff}} = 2\sqrt{2} G_F V_{qb} C_{\text{model}} (\bar{q} \Gamma^\mu b)(\bar{l} \Gamma_\mu \nu), \qquad (1)$$

with $C_{\text{SM}} = 1$ and $\Gamma^\mu = \gamma^\mu P_L$ in the SM, where G_F, V_{qb}, and $P_{L/R}$ denote the Fermi coupling constant, the Cabibbo–Kobayashi–Maskawa [1,2] (CKM) matrix element, and chiral projection operators $(1 \mp \gamma_5)/2$, respectively. Throughout this paper, l indicates all the charged leptons ($l = e, \mu, \tau$), whereas ℓ represents the light charged leptons ($\ell = e, \mu$). Then, the NP effect in the Wilson coefficient (WC) C_{NP},

with an arbitrary Lorenz structure Γ, can be analyzed from the B decay observables.

The exclusive processes of $\bar{B} \to D^{(*)} \ell \bar{\nu}$ and $\bar{B} \to \pi \ell \bar{\nu}$ are used to determine $|V_{cb}|$ and $|V_{ub}|$, respectively. In Ref. [3], the authors extended the fit analysis for the $|V_{cb}|$ determination to include NP effects on the decay distributions with the help of the updated treatment of the form factors [4]. Then, it turns out that non-zero NP contributions with the size of $C_{\text{NP}} \sim \mathcal{O}(\%)$ are possible in the $b \to c \ell \nu$ current, as will be shown later. A similar study for $b \to u \ell \nu$ would be available in future.

On the other hand, the tau modes $\bar{B} \to D^{(*)} \tau \bar{\nu}$ are of particular interest because of the excesses in the experimental measurements of $R_{D^{(*)}} = \mathcal{B}(\bar{B} \to D^{(*)} \tau \bar{\nu})/\mathcal{B}(\bar{B} \to D^{(*)} \ell \bar{\nu})$ compared with the SM predictions. The current measurements are summarized as $R_D^{\text{exp:WA}} = 0.340(27)(13)$ and $R_{D^*}^{\text{exp:WA}} = 0.295(11)(8)$ while several SM predictions are reported, e.g., $R_D^{\text{SM}} = \{0.299(4), 0.297(6), 0.289(4)\}$ and $R_{D^*}^{\text{SM}} = \{0.258(5), 0.245(4), 0.248(1)\}$, where the first ones are from HFLAV [5] and the latter two are from Ref. [3] based on two different sets for the form factors. Then, many studies point out that the excesses can be explained by several types of NP currents in $b \to c \tau \nu$ with $C_{\text{NP}} \sim \mathcal{O}(10\%)$. There also exists the NP study for $b \to u \tau \nu$ as in Ref. [6], and then the typical size of the constraint is $\mathcal{O}(10\%)$ as well.

In light of the above situation, it is natural to ask if we can access such NP effects of $1-10\%$ order at the large hadron collider (LHC) searches. In Ref. [7], τ + missing searches by ATLAS [8] and CMS [9] have been applied to put the LHC bound on C_{NP} in the $b \to c \tau \nu$ current. Then, they found that the current LHC data constrains NP scenarios addressing the $R_{D^{(*)}}$ excesses. See also Refs. [10–16] for the other studies. One can think that the ℓ + missing search by ATLAS with 139 fb^{-1} [17] can probe the LHC bound in $b \to q \ell \nu$ with $q = c, u$ as well.

[a] e-mail: wryou1985@gmail.com (corresponding author)

In this work, we will obtain the LHC bounds for all the possible types of the NP currents in $b \to q l \nu$. *A novel point* of this work is, however, not only for such a comprehensive analysis, but rather for pointing out difference between the Effective-Field-Theory (EFT) and actual NP models, as bellow.

A common outlook on these LHC analyses is that NP constraints are obtained only from a high p_T tail of a SM background (BG) due to a W resonance. To be precise, the transverse mass with $m_T \sim 2–3$ TeV is sensitive to the NP contributions. In this case, the EFT description is not always appropriate for actual NP models, whose effect is usually encoded in $C_{\rm NP}$, as will be shown in this work. We will clarify this point and show that the LHC bound depends on the NP particle mass in the WC.

For this purpose, we focus on NP models with non-resonant m_T distribution, namely, leptoquark (LQ) models. Eventually, we will show that the EFT limit is *not* applicable for the LQ particle mass less than $\mathcal{O}(10)$ TeV due to angular and energy dependence of the charged lepton $l^{\pm}$, which might not much be paid attention so far.

Our paper is organized as follows. In Sects. 2 and 3, we define the model independent NP interactions in $b \to q l \nu$ and the corresponding LQ models, along with the summary of the current flavor bounds. In Sect. 4, we show the m_T distribution of the cross section, and see how the EFT and the LQ model differ at the high p_T tail. Then we present our analysis for the LHC bound on the NP contribution. In Sect. 5, we compare the flavor and LHC bounds, and indicate significance of non-EFT constraints. Finally, our summary and discussion are given in Sect. 6.

2 Effective field theory and flavor bound

In this work, we start with the weak EFT basis Hamiltonian for the semi-leptonic process $b \to q l \nu$:

$$\mathcal{H}_{\rm eff} = 2\sqrt{2} G_F V_{qb} \Big[(1 + C_{V_1}^{ql})(\bar{q}\gamma^\mu P_L b)(\bar{l}\gamma_\mu P_L \nu_l)$$
$$+ C_{V_2}^{ql}(\bar{q}\gamma^\mu P_R b)(\bar{l}\gamma_\mu P_L \nu_l) + C_{S_1}^{ql}(\bar{q}P_R b)(\bar{l}P_L \nu_l)$$
$$+ C_{S_2}^{ql}(\bar{q}P_L b)(\bar{l}P_L \nu_l) + C_T^{ql}(\bar{q}\sigma^{\mu\nu} P_L b)(\bar{l}\sigma_{\mu\nu} P_L \nu_l) \Big] + \text{h.c.}$$
$$\tag{2}$$

Then, the NP contributions are involved in the WCs C_X^{ql} with the SM normalization $2\sqrt{2} G_F V_{qb}$. In this work, we take $|V_{cb}| = 0.0410(14)$ and $|V_{ub}| = 0.00382(24)$ from PDG2020 [18]. We do not consider the right-handed neutrinos.

The B meson decays are described with respect to the WCs at a low energy scale $\mu = m_b$ while a NP model is set at a scale $\mu = \Lambda$. At flavor physics, the EFT limit $q^2 \ll \Lambda^2$

is a good approximation for $\Lambda \gtrsim \mathcal{O}(100)$ GeV. In this case, the corresponding WC is given as

$$2\sqrt{2} G_F V_{qb} C_X(\Lambda) = N_X \frac{h_1 h_2}{M_{\rm NP}^2}, \tag{3}$$

with a mass of a NP particle $M_{\rm NP}$ and its couplings to the SM fermions $h_{1,2}$, and one may typically take $\Lambda = M_{\rm NP}$. The numerical factor N_X depends on the Lorenz structure of the EFT operator. Then, the WCs at these two scales, $C_X(m_b)$ and $C_X(\Lambda)$, are connected by renormalization-group equation (RGE). In this work we follow Ref. [19] for the formula.

Existing flavor bounds on $C_X(m_b)$ are summarized as below.

- $b \to c\ell\nu$: the comprehensive fit analysis [3] of the semi-leptonic processes $\bar{B} \to D^{(*)}\ell\bar{\nu}$ points to non-zero preferred values of the WCs for V_2 and T. The fit along with the form factor leads to $C_{V_2}^{c\ell}(m_b) = +0.02(1), +0.05(1)$ and $C_T^{c\ell}(m_b) = +0.02(1)$ depending on the form factor description. See Ref. [3] for detail.

- $b \to c\tau\nu$: the excesses of the $R_{D^{(*)}}$ measurements have been studied with the EFT approach, and it has been indicating the possibility of NP explanations. Based on the form factor in Ref. [3], we derive updated allowed regions for $C_X^{c\tau}(m_b)$ from the aforementioned latest experimental results, assuming $C_X^{c\ell}(m_b) = 0$. The fit result for each NP scenario can be written as $C_{V_1}^{c\tau}(m_b) = +0.09(3)$, $C_{V_2}^{c\tau}(m_b) = \pm 0.42(7)i$, and $\text{Re}C_T^{c\tau}(m_b) = +0.15(7)$ with $\text{Im}C_T^{c\tau}(m_b)$ to be fixed as ± 0.19. We will also show allowed contour plots on the complex plane later (see Fig. 5) along with the LHC bound. Note that our present analysis excludes the scalar scenarios $S_{1,2}$. In particular, the S_2 solution to the excesses is not consistent with the condition $\mathcal{B}(B_c \to \tau\nu) \lesssim 30\%$, extrapolated from the B_c lifetime [20].[1]

- $b \to u\tau\nu$: there is the NP study for $\bar{B} \to \pi\tau\bar{\nu}$ and $\bar{B} \to \tau\bar{\nu}$ in Ref. [6]. We update the bounds as $C_{V_1}^{u\tau}(m_b) = +0.03(15)$, $C_{V_2}^{u\tau}(m_b) = +0.02(15)$, $C_{S_{1/2}}^{u\tau}(m_b) = 0.00(4), \mp 0.53(4)$, and $C_T^{u\tau}(m_b) = +0.17(25), -0.94(29)$, which are zero-consistent within 1σ, although the latter two have degenerated results.

In addition to them, we also evaluate NP constraints from $B_c \to \ell\nu$ and $B \to \ell\nu$. The former fills missing pieces of the $C_{S_{1,2}}^{c\ell}$ constraints for $b \to c\ell\nu$, while the latter gives the flavor bound for $b \to u\ell\nu$, which is not shown above. Note that these two body decays are not affected by the T operator because of the Lorenz structure.

---

[1] As known well, the S_1 scenario has no solution to the excesses, which results in more than 99.8% CL exclusion.

– The way to derive $\mathcal{B}(B_c \to \tau\nu) \lesssim 30\%$ from the B_c lifetime is indeed independent of the lepton flavor. Therefore, the same condition can be employed to constrain the NP effect in $b \to c\ell\nu$. Given the condition, the electron mode severely constrains the $S_{1,2}$ contributions as $|C_{S_{1,2}}^{ce}(m_b)| < 4 \times 10^{-3}$ due to the chiral enhancement. Similarly, we have $|C_{S_{1,2}}^{c\mu}(m_b)| < 0.8$ from the muon mode. For both lepton modes, the $V_{1,2}$ bounds are very loose.[2]

– The branching ratio of $B \to \mu\nu$ has been measured for the first time, and the result is given as $\mathcal{B}(B \to \mu\nu) = (6.46 \pm 2.22 \pm 1.60) \times 10^{-7}$ [21]. Then, we can obtain $C_{V_{1/2}}^{u\mu} = \pm 0.2(4)$ and $C_{S_{1/2}}^{u\mu} = \pm 3(6) \times 10^{-3}, \mp 35(6) \times 10^{-3}$. On the other hand, the upper limit of the branching ratio for $B \to e\nu$ is so far obtained as $< 9.8 \times 10^{-7}$ (90% CL), which can be compared with the SM value, $(9.8 \pm 1.4) \times 10^{-12}$. Even in this case, the $S_{1,2}$ scenarios are restricted as $|C_{S_{1,2}}^{ue}| < 0.02$.

With the help of these evaluations, we have the exhaustive list of the flavor bounds as in Table 1. These existing and newly evaluated flavor bounds will be compared with the LHC bounds obtained in this work.

3 EFT realizations: leptoquark models

At collider physics, on the other hand, the EFT description is not always applicable. It rather depends on details of the NP model and of the analysis to be used. In this work, we will test the LQ models to see at which scale the EFT limit of Eq. (2) becomes a good approximation for the present and future LHC searches.

The LQ interactions are classified in Ref. [22] with the general $SU(3)_c \times SU(2)_L \times U(1)_Y$ invariant form. In this work, we leave details of the model constructions, and then just consider the explicit interactions only relevant for the present study. In the following subsections, we introduce LQ interactions that generate each operator in Eq. (2). The SM gauge representations for the LQ fields are summarized in Appendix A.

3.1 V_1 operator

The V_1 operator is constructed by the vector leptoquark U_1^μ. The interaction term of interest is written as

$$\mathcal{L}_{V_1} = h_{\mathrm{LQ}}^{ij}\left(\bar{u}_i \gamma_\mu P_L \nu_j + \bar{d}_i \gamma_\mu P_L \ell_j\right)\mathrm{U}_1^\mu + \text{h.c.}, \quad (4)$$

and then the corresponding WC for $b \to q_m \ell_n \bar{\nu}_n$ is obtained as

$$2\sqrt{2}G_F V_{qb} C_{V_1}^{q_m \ell_n} = +\frac{h_{\mathrm{LQ}}^{mn} h_{\mathrm{LQ}}^{*3n}}{M_{\mathrm{LQ}}^2}, \quad (5)$$

for $q_{1,2} = (u, c)$ and $\ell_{1,2,3} = (e, \mu, \tau)$ by performing the Fierz transformation. A similar realization for C_{V_1} is possible by means of the other LQs of S_1, S_3, and U_3^μ as shown in Ref. [23]. See also Appendix B.

3.2 V_2 operator

The V_2 operator is constructed by the scalar leptoquark $\mathrm{R}_2^{2/3}$, where 2/3 denotes the electromagnetic charge. The interaction term

$$\mathcal{L}_{V_2} = \left(h_{\mathrm{LQ}_1}^{ij}\bar{u}_i P_L \nu_j + h_{\mathrm{LQ}_2}^{ij}\bar{d}_i P_L \ell_j\right)\mathrm{R}_2^{2/3} + \text{h.c.}, \quad (6)$$

leads to

$$2\sqrt{2}G_F V_{qb} C_{V_2}^{q_m \ell_n} = +\frac{h_{\mathrm{LQ}_1}^{mn} h_{\mathrm{LQ}_2}^{*3n}}{2M_{\mathrm{LQ}}^2}. \quad (7)$$

Concerning a practical model, we need two $SU(2)$ doublet LQ fields $\mathrm{R}_2 = (\mathrm{R}_2^{5/3} \ \mathrm{R}_2^{2/3})$ and $\mathrm{R}_2' = (\mathrm{R}_2^{2/3} \ \mathrm{R}_2'^{-1/3})$ to construct the SM gauge invariant form, as written in Appendix A. Since the LHC signature for the current process is unchanged, we do not consider such a case.

3.3 S_1 operator

The S_1 operator is constructed by the vector leptoquark U_1^μ such that

$$\mathcal{L}_{S_1} = \left(h_{\mathrm{LQ}_1}^{ij}\bar{u}_i \gamma_\mu P_L \nu_j + h_{\mathrm{LQ}_2}^{ij}\bar{d}_i \gamma_\mu P_R \ell_j\right)\mathrm{U}_1^\mu + \text{h.c.}, \quad (8)$$

and we have

$$2\sqrt{2}G_F V_{qb} C_{S_1}^{q_m \ell_n} = -\frac{2h_{\mathrm{LQ}_1}^{mn} h_{\mathrm{LQ}_2}^{*3n}}{M_{\mathrm{LQ}}^2}. \quad (9)$$

Another realization is given by the V_2^μ LQ [23].

3.4 S_2 and T operators

The S_2 and T operators are always connected due to property of the Fierz transformation. They are constructed by the two scalar leptoquarks $\widetilde{\mathrm{R}}_2^{2/3}$ and $\widetilde{\mathrm{S}}_1$. Note that for $\widetilde{\mathrm{LQ}}$ index of the (quark, lepton) pair is flipped as (lepton, quark) in our

---

[2] It is obtained as $|C_{V_{1,2}}^{c\ell}(m_b)| < \mathcal{O}(100)$. We treat such a case as "unbound" in this paper.

Table 1 Status of applicable flavor bounds. "$| < n|$" means $|C_X| < n$ where those for $C_{S_{1,2}}^{ce,c\mu}$ are the bounds from the theoretical estimates whereas that for $C_{S_{1,2}}^{ue}$ is obtained from the 90% CL upper limit. The results with * indicate that there exist another best fit point outside of $C_X \sim 0$. The $C_T^{c\tau}$ result (**) is given real part by fixing the imaginary part to be $\text{Im} C_T^{c\tau} = \pm 0.19$. See the main text for these details

	V_1	V_2	S_1	S_2	T
C_X^{ce}	–	0.02(1)	$\| < 4 \times 10^{-3}\|$	$\| < 4 \times 10^{-3}\|$	0.02(1)
$C_X^{c\mu}$	–	0.02(1)	$\| < 0.8\|$	$\| < 0.8\|$	0.02(1)
$C_X^{c\tau}$	0.09(3)	$\pm 0.42(7)i$	Excluded	Excluded	0.15(7)**
C_X^{ue}	–	–	$\| < 0.02\|$	$\| < 0.02\|$	–
$C_X^{u\mu}$	0.2(4)	$-0.2(4)$	$3(6) \times 10^{-3}$ *	$-3(6) \times 10^{-3}$ *	–
$C_X^{u\tau}$	0.03(15)	0.02(15)	0.00(4)*	0.00(4)*	0.17(25)*

notation just for our calculating convenience. The single S_2 and T terms are respectively realized from

$$\mathcal{L}_{S_2} = \left(-\tilde{h}_{\text{LQ}_1}^{ji} \bar{\nu}_j P_R d_i^c + \tilde{h}_{\text{LQ}_2}^{ji} \bar{\ell}_j P_L u_i^c \right) \widetilde{\text{S}}_1$$
$$+ \left(\tilde{h}_{\text{LQ}_2}^{ji} \bar{\nu}_j P_R u_i - \tilde{h}_{\text{LQ}_1}^{ji} \bar{\ell}_j P_L d_i \right) \widetilde{\text{R}}_2^{2/3} + \text{h.c.}, \quad (10)$$

with $2\sqrt{2} G_F V_{qb} C_{S_2}^{q_m \ell_n} = -\dfrac{\tilde{h}_{\text{LQ}_1}^{n3*} \tilde{h}_{\text{LQ}_2}^{nm}}{M_{\text{LQ}}^2}, \quad (11)$

and

$$\mathcal{L}_T = \left(-\tilde{h}_{\text{LQ}_1}^{ji} \bar{\nu}_j P_R d_i^c + \tilde{h}_{\text{LQ}_2}^{ji} \bar{\ell}_j P_L u_i^c \right) \widetilde{\text{S}}_1$$
$$- \left(\tilde{h}_{\text{LQ}_2}^{ji} \bar{\nu}_j P_R u_i + \tilde{h}_{\text{LQ}_1}^{ji} \bar{\ell}_j P_L d_i \right) \widetilde{\text{R}}_2^{2/3} + \text{h.c.}, \quad (12)$$

with $2\sqrt{2} G_F V_{qb} C_T^{q_m \ell_n} = +\dfrac{\tilde{h}_{\text{LQ}_1}^{n3*} \tilde{h}_{\text{LQ}_2}^{nm}}{4 M_{\text{LQ}}^2}, \quad (13)$

where u^c and d^c denote charge conjugated quarks. Again, a practical model requires the $SU(2)$ doublet LQ field $\text{R}_2 = (\text{R}_2^{5/3} \ \text{R}_2^{2/3})$.

3.5 Mass scale restriction

The LQ searches have been given by the QCD pair production and the single production channels with subsequent decays into a pair of quark and lepton. Then the recent studies [24–26] obtain the lower limit on the LQ mass as ~ 1.5 TeV by assuming 100% branching ratio for the subsequent decay.

On the other hand, the present high p_T searches with the l + missing events can access a larger LQ mass region since LQs produce non-resonant signals in this case.

Once C_X, at any scale, is given from flavor observables and/or LHC studies, the corresponding LQ mass is restricted as long as the LQ coupling is set not too large for perturbation theory [27]. In Fig. 1, we plot the relation between $C_X(\Lambda)$ and M_{NP} of Eq. (3). The numerical factor N_X is fixed as explained in the legend. The Lorenz structures correspond to $N_{S_1} = 2$; $N_{V_1, S_2} = 1$; $N_{V_2} = 1/2$; and $N_T = 1/4$ for
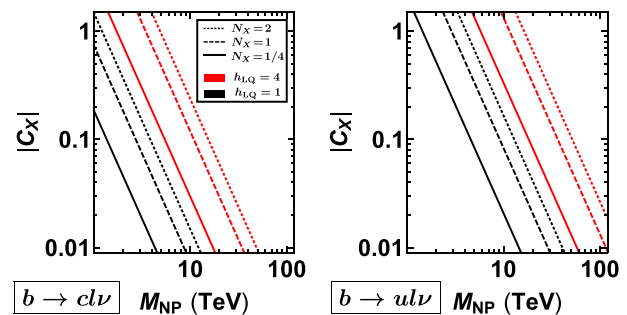

Fig. 1 Relations between the LQ mass and the WC at the NP scale by fixing the LQ coupling

the present LQ models. Then, one can check the accessible LQ mass from the plot. For instance, $|C_X^{cl}(\Lambda)| \sim \mathcal{O}(0.01)$ is produced with $M_{\text{LQ}} \lesssim 10$ TeV for $h_{\text{LQ}} \lesssim 1$ in $b \to cl\nu$. The mass could be $M_{\text{LQ}} \sim 50$ TeV at maximum if we allow the coupling as large as $h_{\text{LQ}} = 4$.

4 Collider study

At the LHC, the EFT operators of Eq. (2) contribute to $pp \to l^\pm + $ missing from $b\bar{q} \to l^- \bar{\nu}$ and $\bar{b}q \to l^+ \nu$ for $q = u, c$. The SM contribution is dominantly given by the $W^\pm$ exchange and generates a resonant structure at $M_{W^\pm}$ in the distribution for the transverse mass

$$m_T = \sqrt{2 p_T^l E_T^{\text{miss}} (1 - \cos \phi_{l\nu})}, \quad (14)$$

where $\phi_{l\nu}$ is the azimuthal angle between l and the missing momentum. On the other hand, the present NP effects are off resonant and widely spread in the m_T distribution. Thus one can expect that a tail of the resonance, namely a larger m_T range, is sensitive to the NP effect.

4.1 EFT limit

To see NP effects on signal event distributions, here we show analytic forms of the parton-level cross sections for $b\bar{c} \to$

$e^-\bar{\nu}$ in the LQ models, and then see the EFT limit of the models. Defining the four momenta as

$$p_c^\mu = E(1, 0, 0, 1), \tag{15}$$

$$p_b^\mu = E(1, 0, 0, -1), \tag{16}$$

$$p_e^\mu = E(1, \sin\theta, 0, \cos\theta), \tag{17}$$

$$p_\nu^\mu = E(1, -\sin\theta, 0, -\cos\theta), \tag{18}$$

we obtain

$$\frac{d\sigma_X}{d\cos\theta} = \frac{1}{3}\frac{|\mathcal{M}_X|^2}{128\pi E^2}, \tag{19}$$

with the spin averaged sum of the squared matrix element, namely $|\mathcal{M}_X|^2$ ($\frac{1}{4}\sum_{\text{spin}}$ is abbreviated), written as

$$|\mathcal{M}_{V_1}^{\text{LQ}}|^2 = 4\,(h_{\text{LQ}}^{21}h_{\text{LQ}}^{31*})^2 E^4 \hat{C}_t^2 (1-\cos\theta)^2, \tag{20}$$

$$|\mathcal{M}_{V_2}^{\text{LQ}}|^2 = (h_{\text{LQ}_1}^{21}h_{\text{LQ}_2}^{31*})^2 E^4 \hat{C}_t^2 (1+\cos\theta)^2, \tag{21}$$

$$|\mathcal{M}_{S_1}^{\text{LQ}}|^2 = 16\,(h_{\text{LQ}_1}^{21}h_{\text{LQ}_2}^{31*})^2 E^4 \hat{C}_t^2, \tag{22}$$

$$\begin{aligned}|\mathcal{M}_{S_2/T}^{\text{LQ}}|^2 = (\tilde{h}_{\text{LQ}_2}^{12*}\tilde{h}_{\text{LQ}_1}^{13})^2 E^4 &\Big[\hat{C}_t^2(1+\cos\theta)^2 \\ &+\hat{C}_u^2(1-\cos\theta)^2 \pm 2\hat{C}_t\hat{C}_u(1-\cos^2\theta)\Big],\end{aligned} \tag{23}$$

where $\hat{C}_t$ and $\hat{C}_u$ involve the LQ propagator written as

$$\hat{C}_t = \left[2E^2(1+\cos\theta) + M_{\text{NP}}^2\right]^{-1}, \tag{24}$$

$$\hat{C}_u = \left[2E^2(1-\cos\theta) + M_{\text{NP}}^2\right]^{-1}. \tag{25}$$

At the EFT limit, the angular and energy dependence of the propagator is suppressed such that $\hat{C}_t \simeq \hat{C}_u \simeq 1/M_{\text{NP}}^2$, and thus we have

$$|\mathcal{M}_{V_1}^{\text{LQ}}|^2 \simeq 4\,\frac{(h_{\text{LQ}}^{21}h_{\text{LQ}}^{31*})^2}{M_{\text{LQ}}^4}E^4(1-\cos\theta)^2, \tag{26}$$

$$|\mathcal{M}_{V_2}^{\text{LQ}}|^2 \simeq \frac{(h_{\text{LQ}_1}^{21}h_{\text{LQ}_2}^{31*})^2}{M_{\text{LQ}}^4}E^4(1+\cos\theta)^2, \tag{27}$$

$$|\mathcal{M}_{S_1}^{\text{LQ}}|^2 \simeq 16\,\frac{(h_{\text{LQ}_1}^{21}h_{\text{LQ}_2}^{31*})^2}{M_{\text{LQ}}^4}E^4, \tag{28}$$

$$|\mathcal{M}_{S_2}^{\text{LQ}}|^2 \simeq 4\,\frac{(\tilde{h}_{\text{LQ}_2}^{12*}\tilde{h}_{\text{LQ}_1}^{13})^2}{M_{\text{LQ}}^4}E^4, \tag{29}$$

$$|\mathcal{M}_{T}^{\text{LQ}}|^2 \simeq 4\,\frac{(\tilde{h}_{\text{LQ}_2}^{12*}\tilde{h}_{\text{LQ}_1}^{13})^2}{M_{\text{LQ}}^4}E^4\cos^2\theta. \tag{30}$$

We can see that the relations of Eqs. (5), (7), (9), (11), (13) are achieved in this limit.

The parton energy E fluctuates in the proton, and thus it is distributed as $0 < E < \sqrt{s}/2$. The energy distribution is weighted with Parton Distribution Function (PDF) according to which b and $\bar{c}$ quarks tend to have low energy. Namely, the distribution in a high energy range is suppressed, and hence the EFT limit is a good approximation even for $M_{\text{NP}} \lesssim \mathcal{O}(1)$ TeV as long as the total cross section is concerned.

However, this is not the case for our analysis. For the present process, the NP sensitivity is gained at large p_T due to the large SM background at lower p_T. In other words, the LHC bound for NP is provided from the signal event distribution with high p_T, which arises from the high energy parton at the cost of the PDF suppression. To be precise, $m_T \sim 2-3\,\text{TeV}(\sim E)$ is the most sensitive for the present case. Therefore, the EFT limit $E^2 \ll M_{\text{NP}}^2$ should be valid only for $M_{\text{NP}} > \mathcal{O}(10)$ TeV.

If $E^2 \lesssim M_{\text{NP}}^2$ is in the case, the angular and energy dependence in the propagator $\hat{C}_t$ and $\hat{C}_u$ is of critical importance since it affects the m_T distribution, as will be seen below.

4.2 Numerical analysis

Here we perform numerical analyses to obtain constraints on the WCs from the $pp \to l^\pm +$ missing searches at the 13 TeV LHC by means of the aforementioned LQ models described in Sect. 3. In this work, we apply numerical setup of the $\ell\nu$ and $\tau\nu$ searches by ATLAS [17] and CMS [9], respectively.

4.2.1 Simulation setup

We generate 100K signal events for every LQ mass $M_{\text{LQ}} = 2, 3, 5, 7.5, 10, 20$, and 100 TeV in each model, by using Madgraph5 [28] with NNPDF2.3 [29] through PYTHIA8 [30] within the five flavor scheme. These generated events are interfaced to DELPHES3 [31] for the fast detector simulation. Then, we apply the following sets of the selection cuts. For the $\ell = e, \mu$ modes, we require $n_\ell = 1$, $p_{T,\ell} > 65$ GeV, $|\eta_\ell| > 2.5$, and $\not{E}_T > 55$ GeV (μ mode), 65 GeV (e mode) following the ATLAS search with 139 fb^{-1} at 13 TeV as in Ref. [17]. Regarding the τ mode, we require exactly one hadronically decaying tau, $n_{\tau_h} = 1$, with $p_{T,\tau} > 80$ GeV and $|\eta_\tau| < 2.1$, no isolated e or μ, $\not{E}_T > 200$ GeV, $0.7 < p_{T,\tau}/\not{E}_T < 1.3$, and $|\Delta\phi(p_\tau, \not{E}_T)| > 2.4$, following the CMS search with 35.9 fb^{-1} at 13 TeV as in Ref. [9].

Figure 2 shows the m_T distributions of $pp \to e^\pm +$ missing for the tensor type NP in the $bu \to e\nu$ mode by fixing $C_T^{ue}(\Lambda_{\text{LHC}}) = 1$, but with different values of M_{LQ} as an illustration. One can see that the distributions converge at the low m_T region, which implies that the EFT limit is valid as it is for the flavor phenomenology. On the other hand, the discrepancy among them at the high m_T region is significant. When the WC is fixed, the more events are expected
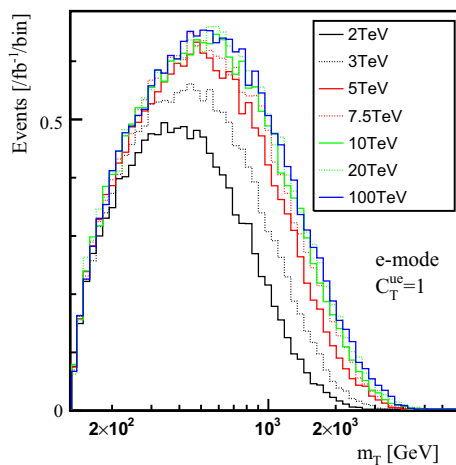
Fig. 2 The simulated m_T distributions of $pp \to e^{\pm}$ + missing for the tensor type NP in the $bu \to e\nu$ mode with $M_{LQ} = 2, 3, 5, 7.5, 10, 20$ and 100 TeV by fixing $C_T^{ue}(\Lambda_{LHC}) = 1$

as M_{LQ} increases, which is because the relative importance of the energy dependent terms in the t/u-channel propagators in Eqs. (24) and (25) is larger for the same m_T value. Similar tendencies are observed for all the type of operators, and also for the $bc \to l\nu$ cases. Regarding the $bc \to l\nu$ cases, however, the size of the discrepancy among the masses are relatively small, since the initial parton contributing to those processes is less energetic c-parton than u-parton. Nevertheless, it generates a significant difference in the LHC bound.

4.2.2 LHC bound on $C_X(\Lambda_{LHC})$

After the event selection cuts, we obtain the m_T distributions and extract the constraints on the WCs based on them. For the e, μ modes, we use the 95% confidence level (CL) upper bounds on the model independent NP contributions of $m_T > m_{T,\min}$, provided in Table 4 and Table 5 of Ref. [17]. We take the $m_{T,\min}$ threshold value providing the strongest constraint for each model. Note that for the electron mode, a deficit of the events in the tale region is observed, which results in stronger constraints than expected. For the τ mode, we perform the same analysis based on the background m_T distribution in Ref. [9]. To be conservative, we assigned a 30–50% systematic uncertainty for $m_{T,\min} = 1.5 - 3$ TeV.

Then, an excluded upper limit on the LQ coupling(s) $h_{LQ_{(i)}}$ is derived for every M_{LQ}. Finally, we translate it into $C_X(\Lambda_{LHC})$. In this work, we fix the LHC scale to be $\Lambda_{LHC} = 1$ TeV for simplicity. Note that we found that the present data is sensitive to the considering NP signal events in the region of $m_T \sim 2 - 3$ TeV.

In Fig. 3, we show the upper bounds on $C_X^{ql}(\Lambda_{LHC})$ at 95% CL with respect to the fixed M_{NP} for all the combinations of

$X = (V_1, V_2, S_1, S_2, T)$, $q = (c, u)$, and $l = (e, \mu, \tau)$. One can clearly see that our results of the LHC bounds depend on the LQ mass for the region of $M_{LQ} < 10$ TeV, while not for the larger LQ mass, as expected. In particular, the lower LQ mass results in the milder LHC bound on the WCs,[3] which is straightforwardly inferred from Fig. 2. We also found that the mass dependence for the T type NP is more significant than one for the other types of NP. This is a non-trivial feature from the angular dependence as in Eq. (23).

One also finds that the EFT results ($M_{LQ} > 10$ TeV) are independent of the chirality of the fermions, and only sensitive to the Lorentz structure. However, this does not hold when the EFT limit is not valid. This is because that the angular and energy dependence in the propagator $\hat{C}_{t,u}$ of Eqs. (20)–(23) affects the m_T distribution.

One may be interested in the LQ scenario with respect to the single $\widetilde{R}_2$ ($\widetilde{S}_1$) LQ particle that generates the relation $C_{S_2} = +4C_T$ ($C_{S_2} = -4C_T$) at the LQ scale in the EFT limit. Indeed, the differential cross section for the $\widetilde{R}_2$ ($\widetilde{S}_1$) scenario is easily derived from Eq. (23) by replacing $\hat{C}_u(\hat{C}_t) \to 0$. Then, we can see that the expression coincides with Eq. (21) of the V_2 operator (Eq. (20) of V_1) by scaling the factor 1 (4) at the EFT limit. Thus, the LHC bounds of these two scenarios, for the e and μ modes, can be read off from those of C_{V_1} and C_{V_2} in Fig. 3. For the τ mode, on the other hand, the τ_L/τ_R difference in the effective operators for $C_{V_{1,2}}$ and $C_{S_2} = \pm 4C_T$ affects the analysis due to the τ decay property at the LHC [37]. We will see this point in Sect. 5.

4.3 Future prospects

In turn, we discuss future sensitivities for the NP searches from $pp \to l^{\pm}$ + missing at the high luminosity (HL)-LHC with 3 ab^{-1} data. Re-scaling the BG information which is used to derive the current bounds including the BG uncertainties, we can obtain the prospect of the HL-LHC bounds on the WCs in Table 2 denoted as "(w/sys)". In the table, the results for the $(2-100$ TeV) mass of the LQ particle are summarized. Since the BG uncertainty in the tail region is significant, we also show the optimistic cases that only the statistic error is taken and the theory uncertainty is controlled (negligible) in future, which is given in "(no sys)" rows.

Furthermore, since the SM background at the tail of the m_T distribution is dominated by the $W^{\pm}$-contribution [9,17], we test S/B improvement by selecting l^- events as explained below. Since the luminosity functions for $u\bar{d}$ and $d\bar{u}$ are not identical but the ratio is $L(u\bar{d})/L(d\bar{u}) \gtrsim 4$ above 2 TeV, the l^+ events are more observed than l^- in the SM. Thus, the ratio

---

[3] For the NP models with a s-channel mediator, e.g. a charged scalar or vector boson, the EFT description usually gives weaker bounds at the LHC, which is opposite to the present case.
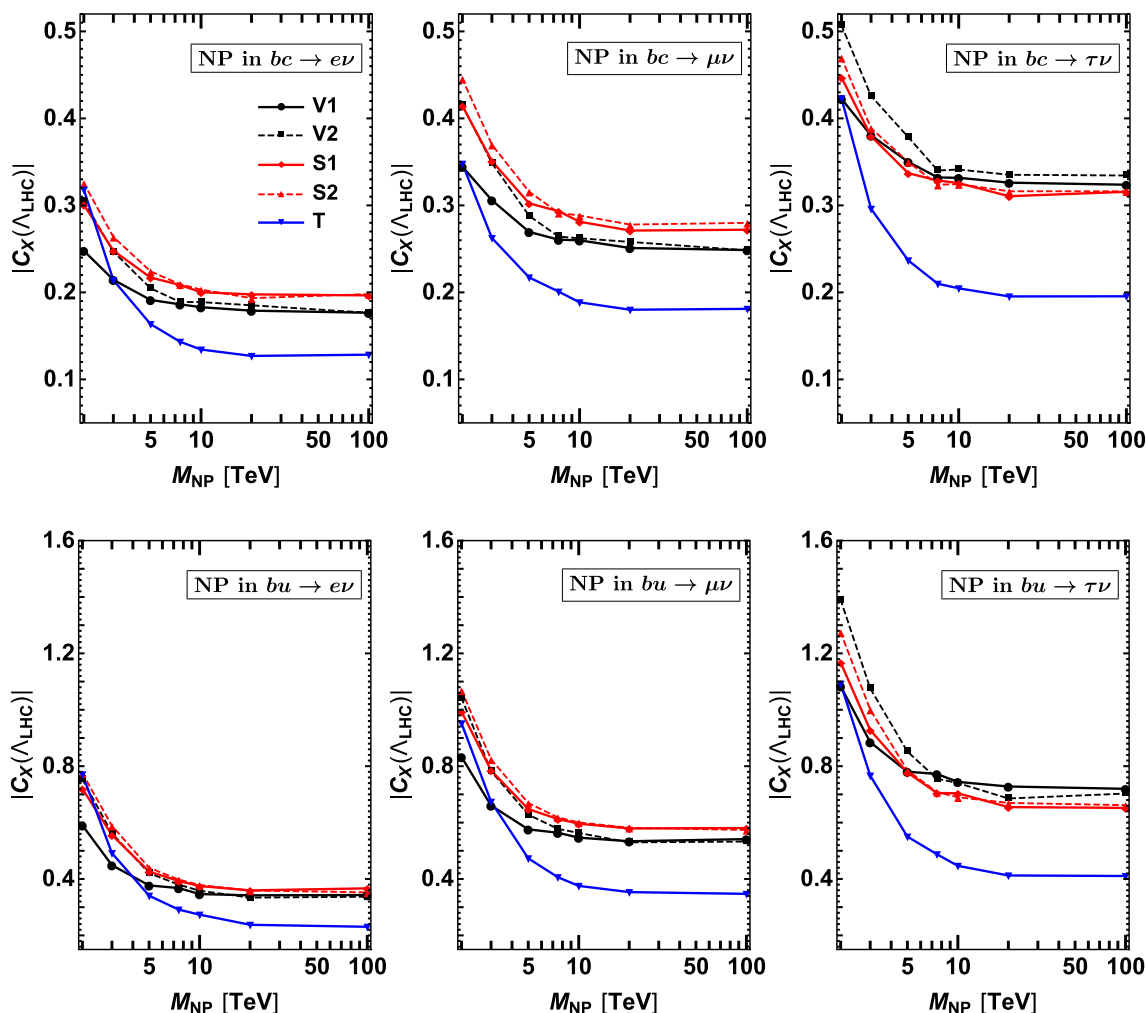
Fig. 3 The 95% CL upper bounds on $C_X^{ql}(\Lambda_{\mathrm{LHC}})$ obtained from the $\ell\nu$ and $\tau\nu$ search data by ATLAS [17] and CMS [9], respectively, where we fix $\Lambda_{\mathrm{LHC}} = 1\,\mathrm{TeV}$

for the l^+/l^- events would be expected as $N_{l^+}/N_{l^-} \gtrsim 4$ in the tail region for the BG contribution. On the other hand, no charge asymmetry is expected between the $c\bar{b}$ and $b\bar{c}$ cases, namely $L(c\bar{b})/L(b\bar{c}) \sim 1$. Therefore, selecting only the l^- events would improve the significance for the $b \to cl\nu$ process. The results by selecting l^- events are given in the "(sys, l^-)" rows, where we assume the BG contributions reduced to $1/4$ and the S/B factor would be improved about twice. It turned out that selecting only the l^- events can potentially improve the sensitivity to C_X^{cl} by $30-40\%$ as seen in the table. We have also checked that the effect of the selecting l^- events with the no BG systematic uncertainty. The results are slightly improved but almost the same numbers in the "(no sys)" rows are obtained, thus, not shown in the table. The reason is that in principle the selection cut does not improve $S/\sqrt{B}$ and neither does the resulting sensitivity, if already the BG uncertainty is well controlled. In other words, the S/B improvement by the selection cut minimizes the effect of the BG uncertainty. For the case of the $b \to ul\nu$ process, the signal charge asymmetry turns out to be larger than that for the SM BG due to the large ratio of $L(u\bar{b})/L(\bar{u}b)$. Hence, selecting l^+ is efficient for this case, but the improvement would be limited.

In any case, we think that the charge asymmetry defined as $A_l = (N_{l^+} - N_{l^-})/(N_{l^+} + N_{l^-})$ would be useful for a more dedicated study in (m_T, A_l) distribution.

If the systematic error is well controlled, the m_T bin with a large number of events will determine the bounds, and thus the smaller m_T bin will become more relevant. On the other hand, when the systematic error is large, the bins closer to the tail will be more effective to set the bounds, since the background number of events should be non-negative. We found that the $m_{T,\min}$ value providing the strongest bound lies in $2-3\,\mathrm{TeV}$ even for the HL-LHC. Therefore, the mass

Table 2 Summary of the current LHC bounds with 139 fb^{-1}/35.9 fb^{-1} for the ℓ/τ modes, and the future HL-LHC potential with 3 ab^{-1}, for the LQ cases of the (2 TeV$-$100 TeV) masses. Note that the latter case corresponds to the EFT limit. See the main text for the detail

	S_1	S_2	V_1	V_2	T
$C_X^{ce}(\Lambda_{\mathrm{LHC}})$					
Current	0.30–0.20	0.33–0.20	0.25–0.18	0.30–0.18	0.32–0.13
Exp (w/sys)	0.35–0.21	0.37–0.21	0.29–0.19	0.35–0.19	0.37–0.15
Exp (w/sys, l^-)	0.26–0.16	0.27–0.16	0.21–0.14	0.26–0.14	0.26–0.11
Exp (no sys)	0.12–0.09	0.13–0.09	0.10–0.08	0.12–0.08	0.11–0.05
$C_X^{c\mu}(\Lambda_{\mathrm{LHC}})$					
Current	0.41–0.27	0.45–0.28	0.34–0.25	0.42–0.25	0.35–0.18
Exp (w/sys)	0.34–0.22	0.37–0.22	0.28–0.20	0.34–0.20	0.32–0.14
Exp (w/sys, l^-)	0.24–0.16	0.26–0.17	0.20–0.15	0.25–0.15	0.23–0.10
Exp (no sys)	0.10–0.08	0.11–0.08	0.09–0.07	0.11–0.07	0.10–0.05
$C_X^{c\tau}(\Lambda_{\mathrm{LHC}})$					
Current	0.45–0.32	0.47–0.32	0.42–0.32	0.51–0.33	0.42–0.20
Exp (w/sys)	0.41–0.20	0.43–0.22	0.38–0.19	0.48–0.25	0.48–0.15
Exp (w/sys, l^-)	0.30–0.18	0.32–0.18	0.28–0.18	0.35–0.19	0.35–0.12
Exp (no sys)	0.13–0.10	0.13–0.10	0.12–0.10	0.14–0.10	0.09–0.06
$C_X^{ue}(\Lambda_{\mathrm{LHC}})$					
Current	0.72–0.37	0.77–0.35	0.59–0.34	0.75–0.34	0.77–0.23
Exp (w/sys)	0.78–0.38	0.84–0.37	0.66–0.36	0.82–0.35	0.91–0.25
Exp (no sys)	0.33–0.20	0.36–0.20	0.27–0.19	0.34–0.19	0.29–0.12
$C_X^{u\mu}(\Lambda_{\mathrm{LHC}})$					
Current	0.99–0.58	1.07–0.57	0.83–0.54	1.04–0.53	0.95–0.35
Exp (w/sys)	0.81–0.45	0.86–0.44	0.67–0.42	0.84–0.41	0.83–0.27
Exp (no sys)	0.27–0.18	0.29–0.18	0.22–0.17	0.28–0.17	0.25–0.11
$C_X^{u\tau}(\Lambda_{\mathrm{LHC}})$					
Current	1.17–0.65	1.27–0.66	1.08–0.72	1.39–0.70	1.09–0.41
Exp (w/sys)	0.88–0.31	0.95–0.30	0.87–0.35	1.05–0.34	1.15–0.22
Exp (no sys)	0.36–0.23	0.39–0.23	0.33–0.24	0.42–0.24	0.29–0.14

dependence will remain important, as long as the systematic error is non-negligible.

The detailed statistical analysis procedures for the future prospects are as follows. For each threshold bin i, we compute the value of S_i^{95} based on the Poisson distribution satisfying the following criteria.

$$\int_0^{B_i^0} dB_i\, f(B_i)\, P(S_i^{95} + B_i, N_{i,\mathrm{BG}}) = 0.05, \qquad (31)$$

where $P(S, N)$ is the probability to observe N or less based on Poisson distribution of S, and $f(B_i)$ is the probability distribution of B_i, the BG contribution for the threshold bin i, and taken as the Gaussian distribution with B_i^0 and ΔB_i restricted to be in the range of $0 \leq B_i \leq B_i^0$, where the normalization is taken as $\int_0^{B_i^0} dB_i\, f(B_i) = 1$. We take the observed number $N_{i,BG}$ in future as the most frequent value

based on the BG distribution. Based on the above procedure, the corresponding upper bound C_X at 95% CL for the each threshold bin i is obtained. The minimum value among i is taken as the 95% CL upper bound of C_X.

Another possibility for future NP searches is to utilize the pseudo rapidity distribution. We discuss it at length in Appendix B.

5 Combined constraints on $C_X(m_b)$

Here we summarize all the constraints on the WCs at the low energy scale $\mu = m_b$ both from the LHC and flavor bounds evaluated in this work.

The RGE running effect of C_X from $\Lambda_{\mathrm{LHC}} = 1$ TeV to $m_b = 4.2$ GeV is numerically presented as
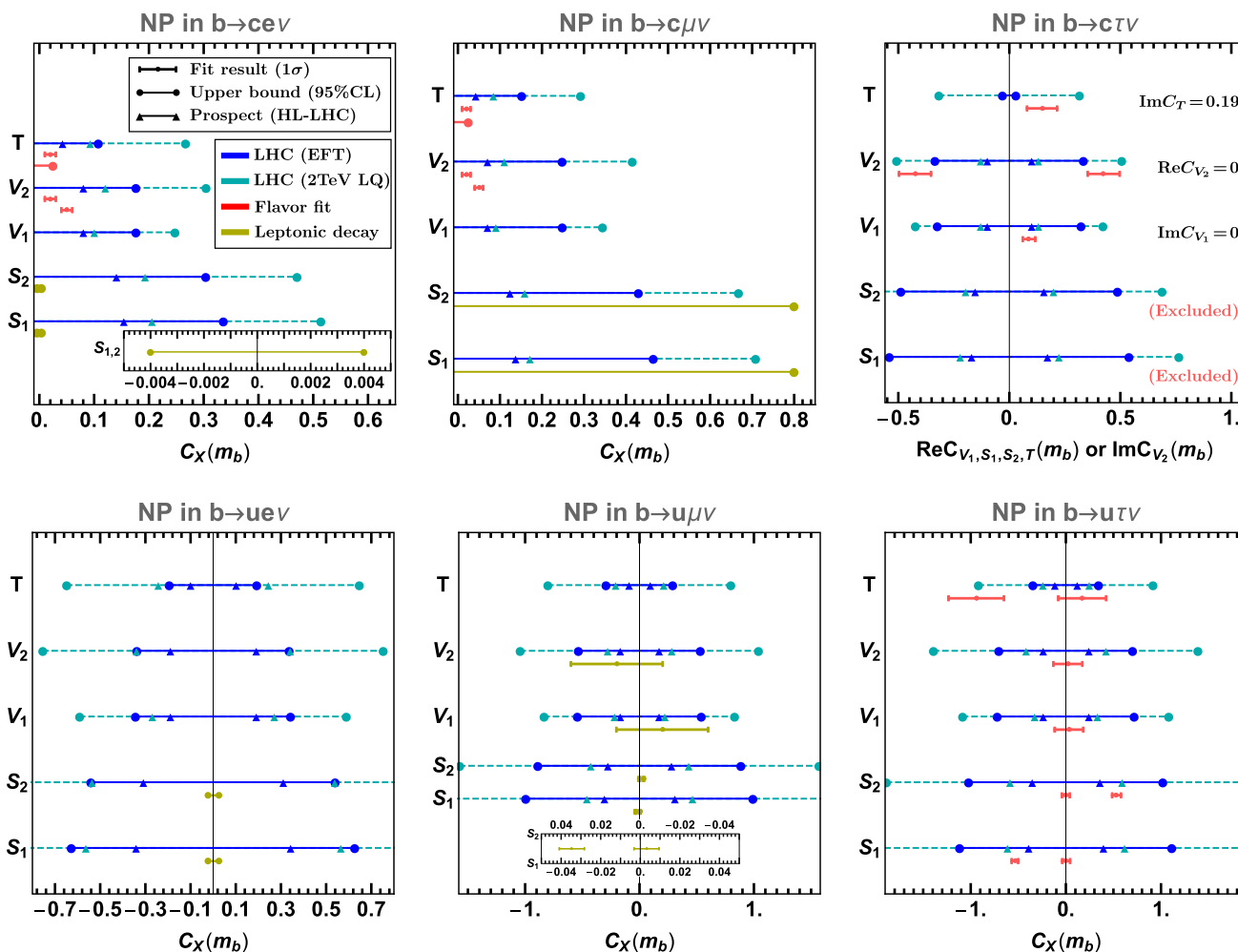
Fig. 4 Summary of the flavor and LHC bounds of the WCs at $\mu = m_b$ along with the future prospects at the HL-LHC with 3 ab^{-1} from Table 2. Unless the flavor bound indicates a favored direction on the complex plane, the WC is taken as real. Note that the prospect for Re $C_T^{c\tau}$ cannot be drawn since the assumption Im $C_T^{c\tau} = 0.19$ already exceeds the result

$$\begin{pmatrix} C_{V_1}(m_b) \\ C_{V_2}(m_b) \\ C_{S_1}(m_b) \\ C_{S_2}(m_b) \\ C_T(m_b) \end{pmatrix} \simeq \begin{pmatrix} 1 & 0 & 0 & 0 & 0 \\ 0 & 1 & 0 & 0 & 0 \\ 0 & 0 & 1.71 & 0 & 0 \\ 0 & 0 & 0 & 1.71 & -0.27 \\ 0 & 0 & 0 & 0 & 0.84 \end{pmatrix} \begin{pmatrix} C_{V_1}(\Lambda_{\mathrm{LHC}}) \\ C_{V_2}(\Lambda_{\mathrm{LHC}}) \\ C_{S_1}(\Lambda_{\mathrm{LHC}}) \\ C_{S_2}(\Lambda_{\mathrm{LHC}}) \\ C_T(\Lambda_{\mathrm{LHC}}) \end{pmatrix},$$

(32)

independent of the (ql) index by following the formula in Ref. [19], (see, also Refs. [32–34]). Hence, the LHC bounds of $C_X^{ql}(m_b)$ are easily obtained by rescaling our results in Fig. 3. The S_2-T mixing propagates $C_{S_2}(\Lambda_{\mathrm{LHC}})$ and $C_T(\Lambda_{\mathrm{LHC}})$ to $C_{S_2}(m_b)$.

Regarding the flavor bounds, we derived the updated values as written in Sect. 2 with the use of the recent experimental data and theoretical input [5,18,35].

In Fig. 4, we show the LHC and flavor bounds on $C_X^{ql}(m_b)$ for $q = (c, u)$ and $l = (e, \mu, \tau)$. The LHC bounds at 95% CL for the EFT (valid for $M_{\mathrm{LQ}} > 10$ TeV) and the $M_{\mathrm{LQ}} = 2$ TeV

LQs are displayed in blue and cyan, respectively. Regarding the flavor bounds, the WC constraints from the semi-leptonic and leptonic processes are given in red and yellow, respectively. The WCs are taken as real unless there exists a specific direction on the complex plane of the WC, favored by the flavor bound such as $C_{V_2}^{c\tau}(m_b)$ and $C_T^{c\tau}(m_b)$. Note that the "fit results" (best point with 1σ uncertainty) are distinguished from the "upper limit" in the figure. Comments are written as follows.

- $b \to c\ell\nu$: the NP effect on this process is significant since the $|V_{cb}|$ measurement is probed from the distribution data of the process. According to the previous analysis in Ref. [3], non-zero NP contributions of $C_{V_2,T}^{c\ell}(m_b)$ are possible at 1–2σ significance as shown in the figure. The scalar scenarios for the electron mode are very restricted from the requirement of $\mathcal{B}(B_c \to e\nu) < 30\%$ while those for muon mode are less constrained. The present
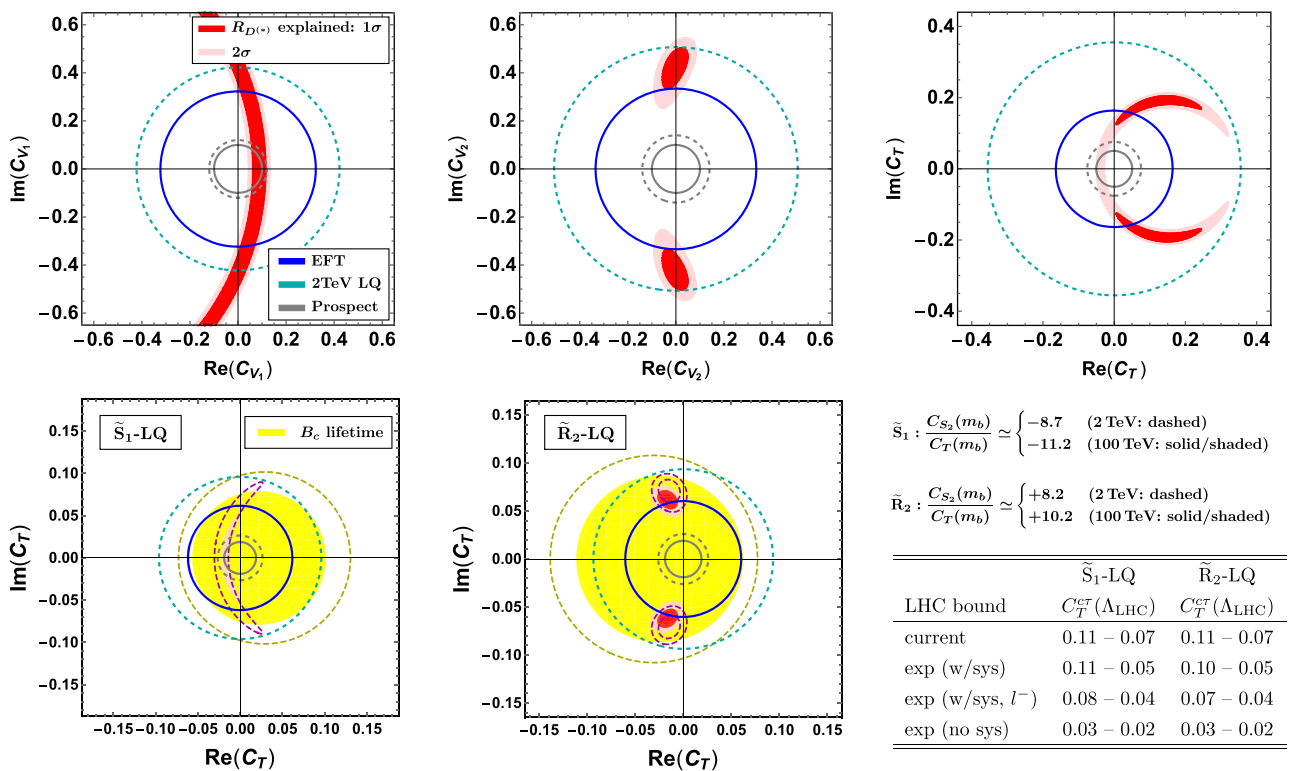
$$\widetilde{S}_1 : \frac{C_{S_2}(m_b)}{C_T(m_b)} \simeq \begin{cases} -8.7 & (2\,\mathrm{TeV: dashed}) \\ -11.2 & (100\,\mathrm{TeV: solid/shaded}) \end{cases}$$

$$\widetilde{R}_2 : \frac{C_{S_2}(m_b)}{C_T(m_b)} \simeq \begin{cases} +8.2 & (2\,\mathrm{TeV: dashed}) \\ +10.2 & (100\,\mathrm{TeV: solid/shaded}) \end{cases}$$

	$\widetilde{S}_1$-LQ	$\widetilde{R}_2$-LQ
LHC bound	$C_T^{c\tau}(\Lambda_{\mathrm{LHC}})$	$C_T^{c\tau}(\Lambda_{\mathrm{LHC}})$
current	$0.11 - 0.07$	$0.11 - 0.07$
exp (w/sys)	$0.11 - 0.05$	$0.10 - 0.05$
exp (w/sys, l^-)	$0.08 - 0.04$	$0.07 - 0.04$
exp (no sys)	$0.03 - 0.02$	$0.03 - 0.02$

Fig. 5 The $R_{D^{(*)}}$ favored region (red: 1σ/light-red: 2σ) on the complex plane of $C_X^{c\tau}$ superimposing the LHC bounds at 95% CL for the EFT, 2 TeV LQ, and future prospects shown in blue, cyan, and gray, respectively. The left/middle/right panel is for the $V_1/V_2/T$ scenario (upper), while the left/middle for the single $\widetilde{S}_1/\widetilde{R}_2$ scenario and right for their LHC bounds (lower)

LHC bounds generally look milder than the flavor ones. However, we can see that the results for C_T^{ce}, $C_T^{c\mu}$, and $C_{S_{1,2}}^{c\mu}$ are well competitive.

- $b \to c\tau\nu$: the current $R_{D^{(*)}}$ excesses are explained by the V_1, V_2, and T scenarios as shown in the red bars, and the LHC bounds are very comparable to these flavor-favored regions. Our constraints in the EFT limit are weaker than that of Ref. [7] but consistent with Ref. [16]. Then, it is quite significant whether the EFT limit is applicable or not to the corresponding LQ model. In particular, we found that the V_2 and T solutions to the excesses are almost excluded by the LHC bounds in the EFT limits whereas these scenarios are still allowed in the LQ models with $M_{\mathrm{LQ}} = 2$ TeV. For the scalar scenarios, see Sect. 2.
- $b \to u\ell\nu$: At present, the flavor bound is available only from $B \to \ell\nu$. For both the electron and muon modes, the scalar scenarios with $|C_{S_i}^{u\ell}| \lesssim \mathcal{O}(0.01)$ are allowed from the flavor bound, which is much severer than the LHC bound. Regarding the vector scenarios, on the other hand, the flavor and LHC bounds are comparable for the muon mode. Note that the other NP scenarios, $C_{V_{1,2},T}^{ue}$ and $C_T^{u\mu}$, are more constrained from our LHC study than the leptonic processes. See also Ref. [36]. A comprehensive

fit analysis for $B \to (\pi, \rho, a_1)\ell\bar\nu$ in the presence of the NP effects for the flavor bound would be our future work.
- $b \to u\tau\nu$: the LHC bounds are loose, naively given as $|C_X^{u\tau}(m_b)| \lesssim \mathcal{O}(1)$. Nevertheless, the LHC bound is already significant for the tensor scenario, which excludes a part of the allowed regions from the flavor bound. We can also confirm importance of the non-EFT case as well as the other currents.

We also present the maximum reaches at the HL-LHC in the "no sys" scenario of Table 2 for comparison. As seen, we clarified the significance of the HL-LHC sensitivity for the NP scenarios. For instance, the V_2 and T solutions to the current $R_{D^{(*)}}$ excesses can be excluded.

We note that the mass of the NP model, namely LQ for the present case, is theoretically restricted apart from the above bounds. For instance, once we employ the unitarity bound for NP in $b \to c\tau\nu$ to explain the $R_{D^{(*)}}$ excesses, the NP mass is restricted as $\lesssim 9$ TeV [27].[4] If this is the case, the EFT description is no longer appropriate for the LHC analysis with the high p_T tail, but it provides the overestimated bound. To be precise, the EFTs with $V_{1,2}$ and $S_{1,2}$ types give $> 30\%$ ($\sim 10\%$) severer LHC bounds than the corresponding LQ cases

---

[4] A loose restriction is obtained from Fig. 1.

with $m_{LQ} \sim 2\,(5)$ TeV. As for the T type, the EFT – 2 TeV LQ difference is much larger as seen in Fig. 4. Therefore, our non-EFT study is of critical importance and useful for practical NP scenarios with a NP mediator mass of $\mathcal{O}(1)$ TeV.

Lastly, in Fig. 5, we provide the favored regions on the complex plane of $C_X^{c\tau}(m_b)$ to explain the $R_{D^{(*)}}$ excesses and compare it with the current and prospect LHC bounds. The single $\widetilde{R}_2$ and $\widetilde{S}_1$ scenarios are also presented here since they also have the solution. Note that the ratio C_{S_2}/C_T at the m_b scale varies for the different LQ mass, which affects the allowed region.[5] One finds that the $\widetilde{R}_2$ solution is almost excluded by the LHC bound for the EFT case whereas it is still viable for $M_{LQ} \gtrsim 2$ TeV. For both cases, the HL-LHC could test this scenario. We can also see that the LHC bound for the $\widetilde{R}_2$ $(\widetilde{S}_1)$ scenario in terms of C_T is a bit severer than what is translated from that for the V_2 (V_1) operator by $C_{V_{2(1)}} \to 4C_T$ (unlike the e and μ cases, mentioned in Sect. 4.2.2). This is due to the fact [37] that the fraction of τ_R to the visible τ decay is larger than that of τ_L at the LHC. Thus, by determining the τ polarization we can distinguish a model that forms the V_2 (V_1) operator from $\widetilde{R}_2$ $(\widetilde{S}_1)$ that generates S_2-T, although these two have (almost) the same 2 to 2 scattering kinematics. A similar feature can be seen in measuring the τ polarization of $\bar{B} \to D^{(*)}\tau\bar{\nu}$ at Belle II, which could distinguish the type of LQ responsible for the $R_{D^{(*)}}$ excesses, see, e.g., Ref. [19].

We can conclude that one could discover the NP signal even for a heavier LQ mass of $\sim \mathcal{O}(10)$ TeV, if the $R_{D^{(*)}}$ excesses are truly caused by the NP contribution. Otherwise, these NP scenarios will be excluded.

6 Summary and discussion

With the help of the recent development for the $\bar{B} \to D^{(*)}$ form factors, the flavor fit analysis for the $|V_{cb}|$ determination has indicated possibilities of the non-zero NP contributions to the $b \to c\ell\nu$ current. On the other hand, the experimental excesses for the $R_{D^{(*)}}$ measurements have been implying an indirect NP evidence in the $b \to c\tau\nu$ current. A similar study regarding the $b \to u\ell\nu$ current also obtains upper limits on the NP effects. These situations naturally attract us to direct searches at the LHC.

In this paper, we have considered both the Effective-Field-Theory description and the leptoquark models for all the types of the NP currents in $b \to q\ell\nu$ for $q = (c, u)$ and $l = (e, \mu, \tau)$, and then obtained the comprehensive flavor and LHC bounds with respect to the Wilson coefficients C_X^{ql} defined as in Eq. (2).

The $l^\pm$ + missing searches have been applied for this purpose, where the high p_T tail of the SM background can be

used to obtain the NP constraints. A significant point is that the EFT description is not always valid to constrain the actual NP models from the present LHC searches, since the NP sensitivity is gained from the transverse mass distribution at $m_T \sim 2$–3 TeV, and therefore the EFT limit breaks down for the NP mass to be the same order of the m_T bin. We have shown the clear mass dependence of the m_T distribution in the LQ model for the fixed WC as in Fig. 2.

Our investigation is based on the ATLAS [17] and CMS [9] analyses for $l = (e, \mu)$ and $l = \tau$, respectively. The LHC bounds of our results are summarized in Fig. 3 and Table 2. Then, we have seen the LQ mass dependence on the LHC bounds. Furthermore, we have confirmed that the EFT limit is a good approximation for $M_{LQ} \gtrsim 10$ TeV, while the vector and scalar type EFTs provide $> 30\%$ ($\sim 10\%$) overestimated bounds for the smaller mass of $\sim 2(5)$ TeV. Regarding the tensor type, the difference is much larger such as $> 60\%$.

We have also evaluated potential of the $l^\pm$ + missing searches at the HL-LHC with 3 ab^{-1}, and then obtained the future projections of the HL-LHC sensitivity. Then we found that selecting only the l^- events can potentially improve the sensitivity to C_X^{cl} by 30–40%. We conclude that the maximum reaches for the WC sensitivity at the HL-LHC are $|C_X^{cl}| \sim 0.1$ and $|C_X^{ul}| \sim 0.1$–0.3 mostly independent of the lepton flavor ($l = e, \mu, \tau$) and of the type of the NP operators ($X = V_1, V_2, S_1, S_2, T$).

Finally, we put the combined summary for the LHC and flavor bounds on the WCs at the low energy scale $\mu = m_b$ in Figs. 4 and 5. For some cases, one finds that the current LHC bounds are comparable with the flavor bounds. Here, we would like to stress again that the LHC bounds for the LQ models become milder in the case $M_{LQ} < 10$ TeV than those for the EFT, which is quite significant for some of the LQ scenarios when comparing it with the flavor bounds. In particular, the V_2, T, and $\widetilde{R}_2$-LQ (that generates the S_2-T mixed operators) type solutions to the $R_{D^{(*)}}$ excesses are almost excluded by the LHC bounds in the EFT limits (which was first pointed out in Ref. [7]) whereas they are still allowed in the LQ models with $M_{LQ} \gtrsim 2$ TeV. This is the remarkable point of our work.

Note that the V_1 type NP effects for e and μ can be absorbed by scaling V_{qb} by $(1+C_{V_1}^{q\ell})$ since the measurements of these processes determine the CKM elements. Thus, it is usually hard to probe their constraints from the flavor observables. On the other hand, the unambiguous bound on $C_{V_1}^{q\ell}$ is obtained at the LHC, thanks to the distinct m_T distribution.

We would like to propose some idea for further improvements on the $l^\pm$ + missing searches as closing remarks. A more dedicated analysis including an additional b-tagging in the $pp \to bl\nu$ mode along with the LQ mass dependence could be effective for the NP study. Studying multi dimensional signal distribution in terms of (m_T, A_ℓ, η) could enhance the NP sensitivity. Therefore, we would encourage

---

[5] For the present cases, $C_{S_2}(m_b)/C_T(m_b) \simeq \{8.2, 10.2\}$ for $\widetilde{R}_2$ with $M_{LQ} = \{2, 100\}$ TeV, while $\simeq \{-8.7, -11.2\}$ for $\widetilde{S}_1$.

both the experimental groups to provide the (m_T, η) distributions for each charge separately.

Data Availability Statement This manuscript has no associated data or the data will not be deposited. [Authors' comment: This work is based on the ATLAS and CMS data from the open sources of Refs. [8,24], and then our result is reproducible for the third party by following the procedure described in this work. Therefore this manuscript has no associated data.]

Appendix A: LQ interactions and representations

Here we put a short summary for the LQ models that can contribute to $b \rightarrow q l \nu$. The $SU(3)_c \times SU(2)_L \times U(1)_Y$ invariant form of the LQ interaction relevant for the present process is written as

$$U_1 : \quad \bar{Q}_L^i \gamma_\mu L_L^j U_1^\mu, \quad \bar{d}_R^i \gamma^\mu \ell_R^j U_1^\mu, \tag{33}$$

$$U_3 : \quad \bar{Q}_L^i \sigma^I \gamma_\mu L_L^j U_1^{\mu,I}, \tag{34}$$

$$V_2 : \quad \bar{d}_R^{c,i} \gamma_\mu (L_L^j \cdot i\sigma_2 V_2^\mu), \quad (\bar{Q}_L^{c,i} \cdot i\sigma_2 V_2^\mu)\gamma_\mu \ell_R^j, \tag{35}$$

$$S_1 : \quad \bar{Q}_L^{c,i} \cdot i\sigma_2 L_L^j S_1, \quad \bar{u}_R^{c,i} \ell_R^j S_1, \tag{36}$$

$$S_3 : \quad \bar{Q}_L^{c,i} \cdot i\sigma_2 \sigma^I L_L^j S_3^I \tag{37}$$

$$R_2 : \quad \bar{u}_R^i (L_L^j \cdot i\sigma_2 R_2), \quad (\bar{Q}_L^i \cdot R_2)\ell_R^j, \tag{38}$$

$$R_2' : \quad \bar{d}_R^i (L_L^j \cdot i\sigma_2 R_2'), \tag{39}$$

where the quantum numbers are assigned as in Table 3. The $SU(2)_L$ doublet fields V_2, R_2, and R_2' are defined as

$$R_2 = \begin{pmatrix} R_2^{5/3} \\ R_2^{2/3} \end{pmatrix}, \quad R_2' = \begin{pmatrix} R_2'^{2/3} \\ R_2^{-1/3} \end{pmatrix}, \quad V_2 = \begin{pmatrix} V_2^{4/3} \\ V_2^{1/3} \end{pmatrix}, \tag{40}$$

Table 3 Quantum numbers of the LQs with $SU(3)_c \times SU(2)_L \times U(1)_Y$ invariant forms

	S_1	S_3	V_2	R_2	R_2'	U_1	U_3
Spin	0	0	1	0	0	1	1
$F = 3B + L$	-2	-2	-2	0	0	0	0
$SU(3)_c$	3*	3*	3*	3	3	3	3
$SU(2)_L$	1	3	2	2	2	1	3
$U(1)_{Y=Q-T_3}$	1/3	1/3	5/6	7/6	1/6	2/3	2/3

by indicating the electric charges for the two components. Given the above forms, we can extract the explicit interaction terms for $b \rightarrow q l \nu$ as shown in the main text. As for S_1 and R_2 that generate C_{S_2} and C_T, we have redefined the LQ fields by taking its conjugate (just for our computation convenience). Note also that we have identified $R_2'^{2/3}$ with $R_2^{2/3}$ in order to obtain C_{V_2} of Eq. (7). In a proper UV theory, however, a $R_2'^{2/3}$-$R_2^{2/3}$ mixing structure should be inevitable, which is beyond the scope of this work.

Appendix B: Angular distribution

In this appendix, we discuss potential of the angular distribution for the NP search from the l + missing process.

At first, a clear picture can be seen in the angular distribution of the observed lepton at the rest frame of the $(l\nu)$ pair as introduced in Sect. 4.1. For instance, the left panel of Fig. 6 shows the $\cos\theta$ distribution of $pp \rightarrow e^\pm$ + missing for NP in $bu \rightarrow e\nu$, where θ is *always* defined as the angle between e^- and $\bar{q}$ (e^+ and q) for $q = u, c$. Then, we see that the NP operator types are distinguishable. It is obvious, however, that such an angle is not directly accessible at the LHC. Note that the $\cos\theta$ distribution is not symmetric even for the intrinsically symmetric ones (S_1, S_2, T) since the η cut rejects a signal event with $\cos\theta \sim 1$.
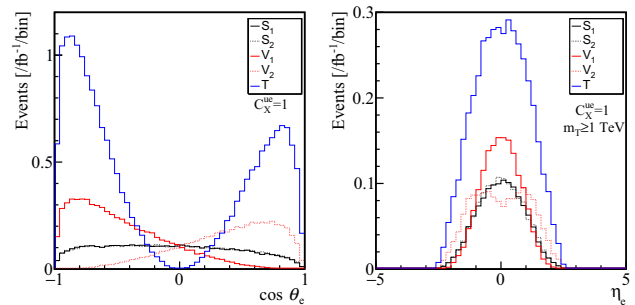

Fig. 6 (Left) The $\cos\theta$ distributions for NPs in the $bu \rightarrow e\nu$ mode with $M_{NP} = 100$ TeV ($C_X = 1$). (Right) The corresponding η_e distributions with the additional cut of $m_T > 1$ TeV

Since the angle information is partially encoded in the measurable pseudo rapidity η, we also show the η-distribution in the right panel of Fig. 6. As a result, the NP effects are degenerate, but we can still say that it is partially distinguishable. For instance, we can access the difference between V_1 and V_2. The difference stems from the fact that u-parton is more energetic than $\bar{b}$-parton while the $\bar{u}$ and b partons are less energetic. In the $bc \rightarrow l\nu$ case, such clear differences are not observed since both $(c, \bar{b})$ and $(\bar{c}, b)$ are less energetic. Note that, for the above evaluation, all the set of the selection cuts and $m_T > 1$ TeV are applied.

References

1. N. Cabibbo, Unitary symmetry and leptonic decays. Phys. Rev. Lett. **10**, 531 (1963)
2. M. Kobayashi, T. Maskawa, CP violation in the renormalizable theory of weak interaction. Prog. Theor. Phys. **49**, 652 (1973)
3. S. Iguro, R. Watanabe, Bayesian fit analysis to full distribution data of $\bar{B} \rightarrow D^{(*)}\ell\bar{\nu}$: $|V_{cb}|$ determination and new physics constraints. JHEP **08**(08), 006 (2020). arXiv:2004.10208 [hep-ph]]
4. M. Bordone, M. Jung, D. van Dyk, Theory determination of $\bar{B} \rightarrow D^{(*)}\ell^-\bar{\nu}$ form factors at $\mathcal{O}(1/m_c^2)$. Eur. Phys. J. C **80**(2), 74 (2020). arXiv:1908.09398 [hep-ph]]
5. Y.S. Amhis et al. (HFLAV), Averages of b-hadron, c-hadron, and τ-lepton properties as of 2018. arXiv:1909.12524 [hep-ex]
6. M. Tanaka, R. Watanabe, New physics contributions in $B \rightarrow \pi\tau\bar{\nu}$ and $B \rightarrow \tau\bar{\nu}$. PTEP **2017**(1), 013B05 (2017). arXiv:1608.05207 [hep-ph]
7. A. Greljo, J Martin Camalich, J .D. Ruiz-lvarez, Mono-τ signatures at the LHC constrain explanations of B-decay anomalies. Phys. Rev. Lett. **122**(13), 131803 (2019). arXiv:1811.07920 [hep-ph]
8. M. Aaboud et al. (ATLAS), Search for high-mass resonances decaying to $\tau\nu$ in pp collisions at $\sqrt{s}$ = 13 TeV with the ATLAS detector. Phys. Rev. Lett. **120**(16), 161802 (2018). arXiv:1801.06992 [hep-ex]
9. A.M. Sirunyan et al. (CMS), Search for a W' boson decaying to a τ lepton and a neutrino in proton–proton collisions at $\sqrt{s}$ = 13 TeV. Phys. Lett. B **792**, 107–131 (2019). arXiv:1807.11421 [hep-ex]
10. B. Dumont, K. Nishiwaki, R. Watanabe, LHC constraints and prospects for S_1 scalar leptoquark explaining the $\bar{B} \rightarrow D^{(*)}\tau\bar{\nu}$ anomaly. Phys. Rev. D **94**(3), 034001 (2016). arXiv:1603.05248 [hep-ph]]
11. W. Altmannshofer, P .S.Bhupal Dev, A. Soni, $R_{D^{(*)}}$ anomaly: a possible hint for natural supersymmetry with R-parity violation. Phys. Rev. D **96**(9), 095010 (2017). arXiv:1704.06659 [hep-ph]
12. S. Iguro, K. Tobe, $R(D^{(*)})$ in a general two Higgs doublet model. Nucl. Phys. B **925**, 560 (2017). arXiv:1708.06176 [hep-ph]
13. M. Abdullah, J. Calle, B. Dutta, A. Florez, D. Restrepo, Probing a simplified, W' model of $R(D^{(*)})$ anomalies using b-tags, τ leptons and missing energy. Phys. Rev. D **98**(5), 055016 (2018). arXiv:1805.01869 [hep-ph]
14. S. Iguro, Y. Omura, M. Takeuchi, Test of the $R(D^{(*)})$ anomaly at the LHC. Phys. Rev. D **99**(7), 075013 (2019). arXiv:1810.05843 [hep-ph]
15. M.J. Baker, J. Fuentes-Martin, G. Isidori, M. Konig, High-p_T signatures in vector 2013 leptoquark models. Eur. Phys. J. C **79**(4), 334 (2019). arXiv:1901.10480 [hep-ph]
16. D. Marzocca, U. Min, M. Son, Bottom-flavored mono-tau tails at the LHC. JHEP **12**, 035 (2020). arXiv:2008.07541 [hep-ph]
17. G. Aad et al. (ATLAS), Search for a heavy charged boson in events with a charged lepton and missing transverse momentum from pp collisions at $\sqrt{s}$ = 13 TeV with the ATLAS detector. Phys. Rev. D **100**(5), 052013 (2019). arXiv:1906.05609 [hep-ex]
18. P.A. Zyla et al. (Particle Data Group), Review of particle physics. PTEP **2020**(8), 083C01 (2020)
19. S. Iguro, T. Kitahara, Y. Omura, R. Watanabe, K. Yamamoto, D^* polarization vs. $R_{D^{(*)}}$ anomalies in the leptoquark models. JHEP **02**, 194 (2019). arXiv:1811.08899 [hep-ph]
20. R. Alonso, B. Grinstein, J.Martin Camalich, Lifetime of B_c^- constrains explanations for anomalies in $B \rightarrow D^{(*)}\tau\nu$. Phys. Rev. Lett. **118**(8), 081802 (2017). arXiv:1611.06676 [hep-ph]
21. A. Sibidanov et al. (Belle), Search for $B^- \rightarrow \mu^-\bar{\nu}_\mu$ decays at the Belle experiment. Phys. Rev. Lett. **121**(3), 031801 (2018). arXiv:1712.04123 [hep-ex]
22. W. Buchmuller, R. Ruckl, D. Wyler, Leptoquarks in lepton-quark collisions. Phys. Lett. B **191**, 442–448 (1987)
23. Y. Sakaki, M. Tanaka, A. Tayduganov, R. Watanabe, Testing leptoquark models in $\bar{B} \rightarrow D^{(*)}\tau\bar{\nu}$. Phys. Rev. D **88**(9), 094012 (2013). arXiv:1309.0301 [hep-ph]
24. A.M. Sirunyan et al. (CMS), Search for a singly produced third-generation scalar leptoquark decaying to a τ lepton and a bottom quark in proton–proton collisions at $\sqrt{s}$ = 13 TeV. JHEP **07**, 115 (2018). arXiv:1806.03472 [hep-ex]
25. M. Aaboud et al. (ATLAS), Searches for third-generation scalar leptoquarks in $\sqrt{s}$ = 13 TeV pp collisions with the ATLAS detector. JHEP **06**, 144 (2019). arXiv:1902.08103 [hep-ex]
26. G. Aad et al. (ATLAS), Search for pairs of scalar leptoquarks decaying into quarks and electrons or muons in $\sqrt{s}$ = 13 TeV pp collisions with the ATLAS detector. JHEP **10**, 112 (2020). arXiv:2006.05872 [hep-ex]
27. L. Di Luzio, M. Nardecchia, What is the scale of new physics behind the B-flavour anomalies? Eur. Phys. J. C **77**(8), 536 (2017). arXiv:1706.01868 [hep-ph]
28. J. Alwall, R. Frederix, S. Frixione, V. Hirschi, F. Maltoni, O. Mattelaer, H.S. Shao, T. Stelzer, P. Torrielli, M. Zaro, The automated computation of tree-level and next-to-leading order differential cross sections, and their matching to parton shower simulations. JHEP **07**, 079 (2014). arXiv:1405.0301 [hep-ph]
29. R.D. Ball, V. Bertone, S. Carrazza, C.S. Deans, L. Del Debbio, S. Forte, A. Guffanti, N.P. Hartland, J.I. Latorre, J. Rojo, M. Ubiali, Parton distributions with LHC data. Nucl. Phys. B **867**, 244–289 (2013). arXiv:1207.1303 [hep-ph]
30. T. Sjostrand, S. Ask, J.R. Christiansen, R. Corke, N. Desai, P. Ilten, S. Mrenna, S. Prestel, C.O. Rasmussen, P.Z. Skands, An introduction to PYTHIA 8.2. Comput. Phys. Commun. **191**, 159–177 (2015). arXiv:1410.3012 [hep-ph]
31. J. de Favereau et al. (DELPHES 3), DELPHES 3, a modular framework for fast simulation of a generic collider experiment. JHEP **02**, 057 (2014). arXiv:1307.6346 [hep-ex]
32. E.E. Jenkins, A.V. Manohar, M. Trott, Renormalization group evolution of the standard model dimension six operators II: Yukawa dependence. JHEP **01**, 035 (2014). arXiv:1310.4838 [hep-ph]
33. R. Alonso, E.E. Jenkins, A.V. Manohar, M. Trott, Renormalization group evolution of the standard model dimension six operators III: gauge coupling dependence and phenomenology. JHEP **04**, 159 (2014). arXiv:1312.2014 [hep-ph]
34. M. Gonzalez-Alonso, J.Martin Camalich, K. Mimouni, Renormalization-group evolution of new physics contributions to (semi)leptonic meson decays. Phys. Lett. B **772**, 777–785 (2017). arXiv:1706.00410 [hep-ph]
35. S. Aoki et al. (Flavour Lattice Averaging Group), FLAG review 2019: flavour lattice averaging group (FLAG). Eur. Phys. J. C **80**(2), 113 (2020). arXiv:1902.0819 [hep-lat]

36. P. Colangelo, F. De Fazio, F. Loparco, Probing new physics with $\bar{B} \to \rho(770) \ell^- \bar{\nu}_\ell$ and $\bar{B} \to a_1(1260) \ell^- \bar{\nu}_\ell$. Phys. Rev. D **100**(7), 075037 (2019). arXiv:1906.07068 [hep-ph]

37. A. Papaefstathiou, K. Sakurai, Determining the helicity structure of third generation resonances. JHEP **06**, 069 (2012). arXiv:1112.3956 [hep-ph]